JOURNAL OF GEOPHYSICAL RESEARCH, VOL. 114, C02016, doi:10.1029/2007JC004466, 2009

Drift and mixing under the ocean surface revisited: Stratified conditions and model-data comparisons

Nicolas Rascle[1,2] and Fabrice Ardhuin[1]

Received 26 July 2007; revised 16 October 2008; accepted 11 November 2008; published 19 February 2009.

[1] A one-dimensional model of the ocean near-surface currents is presented. It includes the enhanced near-surface mixing due to the waves, the wave-induced Stokes drift, the Stokes-Coriolis (SC) effect, and the stratification. Near-surface current shears from this model are compared with the shears of the quasi-Eulerian currents measured using a wave-following platform during the Shelf Mixed Layer Experiment (SMILE). It is shown that the downwind current shears observed during SMILE are well modeled. However, the observed crosswind shears are in poor agreement with the model. The Stokes-Coriolis (SC) term could qualitatively explain this misfit, but it is one order of magnitude too weak. The Ekman-Stokes spiral of the model is compared with the spiral observed during the long time series of measurements Long Term Upper Ocean Study 3. The effects of stratification are taken into account. The mean velocity profiles of the model closely agree with observations. However, there is no evidence of the SC effect on the shape of the observed current profile. The observed profile is found to be a consequence of the current rectification due to the time-varying stratification. The SC effect calculated from a numerical wave hindcast is weak but should have been observed. In fact, it is estimated that the wave-induced bias in the current measurements is larger than the SC effect. Finally, it is shown that the variation of surface drift with wave age, which was estimated to be small in unstratified conditions, is important in the presence of shallow mixed layers.

Citation: Rascle, N., and F. Ardhuin (2009), Drift and mixing under the ocean surface revisited: Stratified conditions and model-data comparisons, *J. Geophys. Res.*, *114*, C02016, doi:10.1029/2007JC004466.

1. Introduction

[2] Breaking waves in the ocean can dramatically enhance near-surface mixing. This wave-induced mixing was established from measurements of turbulent kinetic energy (TKE) dissipation [*Agrawal et al.*, 1992; *Terray et al.*, 1996], and it was also observed in measurements of downwind current vertical shear very close to the surface during the Shelf Mixed Layer Experiment (SMILE) [*Santala*, 1991; *Terray et al.*, 2000]. As a result, the surface mean current is rather weak, around 0.5% of the wind speed at 10 meters U_{10} when the ocean is not stratified and when the waves are developed. This quasi-Eulerian mean current is defined as the Lagrangian drift minus the wave Stokes drift [see *Jenkins*, 1987; *Rascle et al.*, 2006; *Ardhuin et al.*, 2008]. This small quasi-Eulerian drift can be overwhelmed by large surface drift due to the wave Stokes drift (*Rascle et al.* [2006], hereinafter referred to as RAT06), which can be as large as 1.4% of U_{10} [see also *Rascle et al.*, 2008]. Other processes likely contribute to the drift of surface-trapped buoyant objects that reaches 2 to 3% of U_{10} [*Huang*, 1979]. In the presence of stratification, the confinement of the Ekman current near the surface may be an important factor.

[3] Waves are also associated with a Stokes-Coriolis (SC) current [*Hasselmann*, 1970; *Xu and Bowen*, 1994]. Namely, in a rotating frame of reference, a wave-induced stress perpendicular to the wave propagation modifies the profile of the Ekman current. In an inviscid ocean, this stress drives a mean current which compensates the Stokes drift of the waves when averaged over the inertial period. However, in the presence of a strong vertical mixing, this return flow is made vertically uniform. Because the Stokes drift of a wind sea exhibits a strong vertical shear, the return flow only compensates the Stokes drift when vertically integrated over depth, and there is a net drift at every depth. This was shown by RAT06 without any stratification. Does this remain valid if the Ekman current is also confined near the surface, by a shallow mixed layer for instance?

[4] The Stokes-Coriolis effect has been recently observed very close to the shore, in water depths of 10–15 m, from bottom-mounted ADCP's [*Lentz et al.*, 2008]. However, in the open ocean, it has never been clearly observed. Evidence of this effect has been sought by *Lewis and Belcher* [2004] and *Polton et al.* [2005] in the observations of the subsurface Ekman current during Long Term Upper Ocean Study 3 (LOTUS 3) [*Price et al.*, 1987]. Unfortunately, neither the wave-enhanced surface mixing nor the quite shallow diurnal mixed layer during LOTUS 3 have been

[1]Centre Militaire d'Océanographie, Service Hydrographique et Océanographique de la Marine, Brest, France.

[2]Laboratoire de Physique des Océans, Université de Bretagne Occidentale, Brest, France.

0148-0227/09/2007JC004466$09.00

taken into account in their investigations, although they can radically change the interpretation of the observed current profiles [*Price and Sundermeyer*, 1999]. Also, evidence of the Stokes-Coriolis forcing in the open ocean has not been sought yet in measurements much closer to the surface, such as those of SMILE.

[5] The present work builds on the modeling concepts proposed by *Jenkins* [1987] and RAT06. These include a separation of near-surface flow into a wave Stokes drift and a quasi-Eulerian current. A realistic vertical mixing is applied to the quasi-Eulerian current. This physical description leads to a different analysis of the near-surface current measurements depending on whether they are Lagrangian or Eulerian, because the Stokes drift was shown to be of same order as the quasi-Eulerian current. RAT06 performed qualitative comparisons of modeled and observed near-surface quasi-Eulerian currents and of subsurface hodographs, showing encouraging results. However, those comparisons needed further analysis. For instance, the near-surface quasi-Eulerian currents observed during SMILE were only compared to model predictions in the downwind direction, and they took for granted the analysis of *Santala* [1991], even though this analysis was based on questionable assumptions on the structure of the velocity shear (see section 3).

[6] Here the effect of stratification is added to the model presented by RAT06, in order to make a quantitative comparison with the observations of near-surface current, and address the following questions: How well this model can reproduce the vertical shears observed close to the surface, both in the downwind and the crosswind direction? What is the impact of the Stokes-Coriolis effect on the Eulerian and Lagrangian current profiles in shallow mixed layers? Is there any observational evidence of this effect in the observations of Eulerian hodographs? What is the quantitative effect of shallow mixed layers on the surface drift?

[7] The model used for this study is described in section 2. The near-surface shears of the quasi-Eulerian currents observed during SMILE are analyzed in section 3. The Ekman-Stokes spirals from the LOTUS 3 data are analyzed in section 4. Finally, the surface drift of the model in the presence of waves and stratification is discussed in section 5.

2. Model

[8] The model used in the present study can be summarized as follows. Oceanic motions are separated in three components, mean flow, waves and turbulence. Turbulence is separated from other motions by an average over flow realizations for given wave phases. The mean flow and wave motions are then averaged over the wave phases with a generalized Lagrangian mean [*Andrews and McIntyre*, 1978; *Ardhuin et al.*, 2008]. The horizontal total mean momentum $\mathbf{U}$ is split in a quasi-Eulerian mean $\widehat{\mathbf{u}}$ and a Stokes drift,

$$\mathbf{U} = \widehat{\mathbf{u}} + \mathbf{U}_s. \tag{1}$$

Approximated to second order in the wave slope, the vertical profile of Stokes drift is given by the spectrum of the sea surface elevation, used here as a forcing for the model. Following *Ekman* [1905] we assume that the wave, velocity, and turbulent properties are uniform horizontally, which reduces the problem to the vertical dimension.

[9] For the sake of simplicity and because we want to simulate a period of hundreds of days, a simple eddy viscosity model with a TKE closure scheme will be used. This model is adapted from *Craig and Banner* [1994] (see also the work of RAT06). The wave-enhanced near-surface mixing is parameterized by the addition of a TKE flux at the surface, and the specification of a large subsurface roughness length z_0. The extension of this model to a stratified ocean is taken from *Noh* [1996] and the following works [*Noh and Kim*, 1999; *Noh*, 2004]. The effects of stratification on the eddy diffusivities are parameterized via a turbulent Richardson number, where the conversion of TKE to potential energy is made regardless of the origin of this turbulence [*Noh*, 1996]. This model was chosen for its ability to reproduce the diurnal thermocline.

[10] The equations for the quasi-Eulerian horizontal momentum, for the mean buoyancy $B = -g\rho_w/\rho_0$ (g is the gravity acceleration, ρ_w the water density, and ρ_0 a reference density), and for the mean turbulent kinetic energy E are [*Noh and Kim*, 1999]

$$\frac{\partial \widehat{\mathbf{u}}}{\partial t} = -f\mathbf{e}_z \times (\widehat{\mathbf{u}} + \mathbf{U}_s) + \frac{\partial}{\partial z}\left(K\frac{\partial \widehat{\mathbf{u}}}{\partial z}\right), \tag{2}$$

$$\frac{\partial B}{\partial t} = \frac{\partial}{\partial z}\left(K_B\frac{\partial B}{\partial z}\right), \tag{3}$$

$$\frac{\partial E}{\partial t} = \frac{\partial}{\partial z}\left(K_E\frac{\partial E}{\partial z}\right) + K\left(\frac{\partial \widehat{\mathbf{u}}}{\partial z}\right)^2 + K_B\left(\frac{\partial B}{\partial z}\right) - \frac{Cq^3}{l}, \tag{4}$$

where f is the Coriolis parameter, $-f\mathbf{e}_z \times \mathbf{U}_s$ is the Stokes-Coriolis term, $q = \sqrt{2E}$ is the turbulent velocity scale, l is the mixing length, and where we used the eddy viscosity and diffusivity concepts. Those viscosity and diffusivities are parameterized by

$$(K, K_B, K_E) = lq(S, S_B, S_E). \tag{5}$$

The proportionality constants (S, S_B, S_E, C) depend on the stratification via the introduction of a turbulent Richardson number [*Noh*, 2004]

$$Ri_t = \left(\frac{Nl}{q}\right)^2, \tag{6}$$

$$S = 0.39(1 + 5Ri_t)^{-1/2}, \tag{7}$$

$$S_B = S/0.8(1 + 0.5Ri_t)^{1/2}, \tag{8}$$

$$S_E = S/1.95, \tag{9}$$

$$C = 0.39^3(1 + 5Ri_t)^{1/2}, \tag{10}$$

where N is the Brunt-Väisälä frequency ($N^2 = -\partial B/\partial z$). Note that all proportionality constants (S, S_B, S_E, C) depend on the turbulent Richardson number Ri_t and that the buoyancy diffusivity is multiplied by a Prandtl number which also depends on Ri_t.

[11] The mixing length is parameterized as

$$l = \frac{\kappa(z_0 - z)}{1 + \kappa(z_0 - z)/h}, \tag{11}$$

where $\kappa = 0.4$ is the von Kármán's constant, h is the mixed layer depth, defined as the depth where the TKE is reduced by four orders of magnitude compared to its surface value [*Noh*, 2004], and z_0 is the roughness length. We use $z_0 = 1.6$ H_s as in the work of *Terray et al.* [2000]. H_s is the significant wave height of the wind sea, a proxy for the scale of the breaking waves that are responsible for the mixing.

[12] The boundary conditions at the surface ($z = 0$) are

$$K \frac{\partial \hat{\mathbf{u}}}{\partial z}\bigg|_{z=0} = u_*^2, \tag{12}$$

$$K_B \frac{\partial B}{\partial z}\bigg|_{z=0} = Q \tag{13}$$

$$K_E \frac{\partial E}{\partial z}\bigg|_{z=0} = \Phi_{oc}, \tag{14}$$

where u_* is the waterside friction velocity, related to the wind stress τ by $\tau = \rho_w u_*^2$, Q is the surface downward buoyancy flux, and Φ_{oc} is the surface downward TKE flux. Following *Terray et al.* [1996], the TKE flux is parameterized as $\Phi_{oc} = \alpha u_*^3$, with $\alpha = 100$.

[13] The bottom has almost no effect on the near-surface dynamics, provided that the depth is substantially greater than both Stokes and Ekman depths and than the mixed layer depth. Therefore the bottom boundary layer is not described here.

[14] Equations (2)–(4) are solved with a time step of dt = 10 s and a vertical discretization of dz = 1 m. Each variable are collocated, the space differentials are expressed in standard second-order centrally differenced forms, and the time step is implicit.

[15] The use of such a simple eddy viscosity model is justified by the reasonable agreement with the velocity profiles of more sophisticated models like the large eddy simulations (LES) of *McWilliams et al.* [1997] or *Noh et al.* [2004], as discussed for instance by *Kantha and Clayson* [2004].

3. Analysis of the Near-Surface Shears: The SMILE Data

3.1. Experiment

[16] The SMILE experiment was described in details by *Santala* [1991] and only a short review will be given here. The experiment took place on the northern California shelf in 1988–1989. It included measurements of oceanographic and atmospheric variables using moored platforms. One measurement of particular interest was made with the Surface Acoustic Shear Sensor (SASS), a wave-following device which included velocity measurements very close to the surface, at depths smaller than H_s. In our analysis, we will focus on those SASS measurements, ignoring the longer and deeper measurements from conventional moorings made during the same field experiment, and we will use the abbreviation SMILE to refer to the SASS measurements only. The SASS buoy is a rigid array designed specifically to follow the surface elevation. It was moored over the shelf in 90-m depth, at the location (38°39′N, 123°29′W). Currents relative to the buoy were measured at depths 1.11, 2.51, 3.11, and 5.85 m using 4 acoustic current meters. Gyroscopes and accelerometers were used to determine the motion of the buoy relative to the inertial frame of reference. The resulting measurements of currents referred to the inertial frame are unique with respect to their proximity of the surface. Horizontal average velocities were corrected for a wave-induced bias due to correlations between the SASS motion and the wave orbital velocities, estimated from measured wave spectra (see also section 4.6 for a physical description of the wave-induced bias). The velocities were also corrected for estimated errors due to flow distortions induced by the structure.

[17] Here we focus on 13 records averaged over 40 mn, spread during the afternoon and night on 27 February 1989. The average wind speed was U_{10} = 13.6 m s^{-1} and the average wave height was H_s = 2.3 m, both approximately aligned (from the northwest, 300°) and steady. The wave peak period was T_p = 7.8 s, which corresponds to a wave age C_p/U_{10} = 0.89, where C_p is the wave phase speed at the spectral peak. The combined measurements of temperature with the SASS and with the nearby conventional mooring show that water column was unstratified down to 20-m depth. To parameterize the atmospheric boundary layer, *Santala* [1991] used local observations and extrapolated missing observations, such as the air temperature, from distant buoy measurements. He calculated the stability parameter $-\kappa Z/L$ [*Large and Pond*, 1981], where Z = 7 m is the elevation above the sea surface and $L = u_*^3/Q$ the Monin-Obukhov length scale, and he obtained values between 0 and −0.03. The corresponding downward surface heat flux Q_h is thus between 0 and −90 W m^{-2}. Using a similar combination of in situ measurements and bulk formulae, *Beardsley et al.* [1998] found that the shortwave heat flux roughly compensated the longwave, latent, and sensible heat loss, giving a small daily mean surface heat flux on 27–28 February, around +30 W m^{-2} (given the uncertainty of visual reading of *Beardsley et al.* [1998], Figure 6). We will thus neglect this small heat flux, given the large values of the Monin-Obukhov length scale (93 m).

3.2. Model

[18] The model is run with the steady observed mean wind speed. The wind stress is calculated from the wind speed using the parameterization of *Charnock* [1955], which gives u_* = 0.0186 m s^{-1}. The temperature is initialized with the observed stratification, with a thermocline around 20 m, and a zero surface heat flux is used. The Stokes drift, needed to compute the Stokes-Coriolis force, is estimated by assuming that the sea state conforms to a JONSWAP spectrum

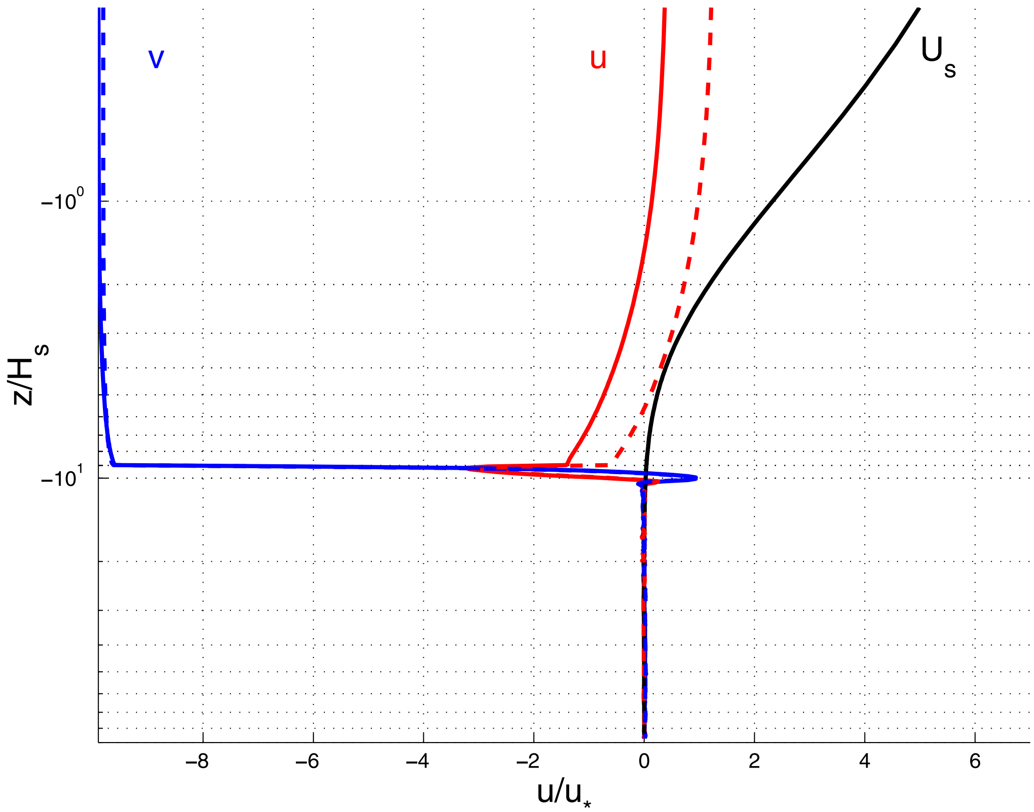

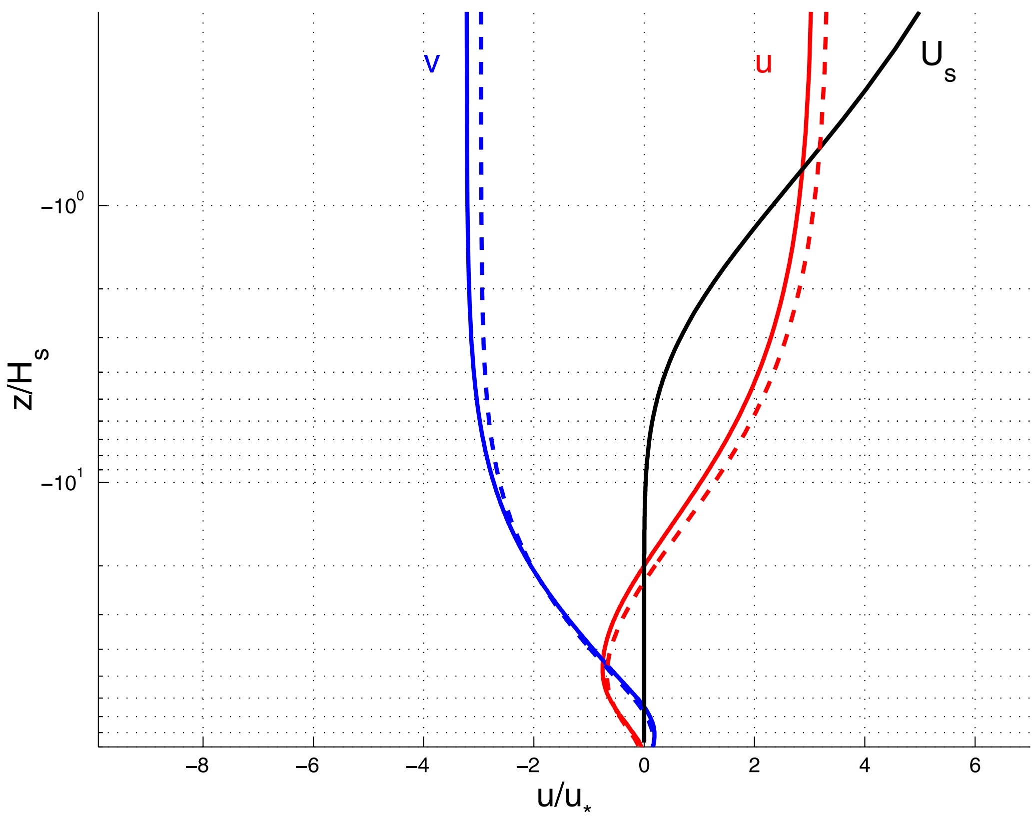

Figure 1. Velocity profiles from the model. $\widehat{u}$ is the downwind quasi-Eulerian velocity, $\widehat{v}$ is the crosswind quasi-Eulerian velocity, and U_s is the Stokes drift. Velocities and elevation are normalized by the waterside friction velocity u_* and by the significant wave height H_s, respectively. Solid lines and dashed lines are model results with and without the Stokes-Coriolis effect, respectively. (top) With a 20-m−deep mixed layer as observed during SMILE. (bottom) Without the effect of stratification.

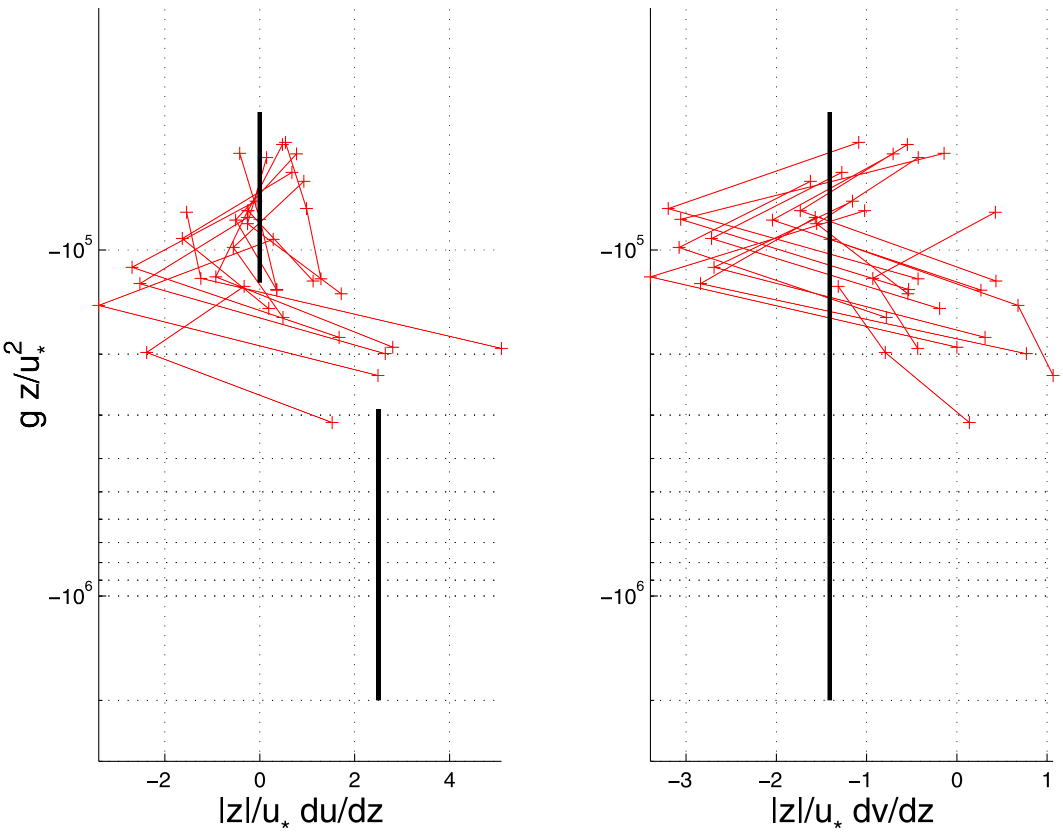

Figure 2. Plot similar to Figures 7–5 of *Santala* [1991], but for the SASS data only. Nondimensional variation of shear with depth for the (left) downwind and for the (right) crosswind directions. The plus symbols and thin lines are measurements from the SASS, the thick solid lines are the shears inferred in the original analysis of *Santala* [1991], with the three-layer structure in the downwind direction.

[*Hasselmann et al.*, 1973; *Kudryavtsev et al.*, 1999], with a fetch of 100 km which gives the observed H_s. The peak period of waves is slightly underestimated with this method, giving T_p = 6.4 s whereas 7.8 s was observed. The Stokes transport of the waves, important to measure the magnitude of the Stokes-Coriolis force, might then be overestimated. The model results, averaged over one inertial period, are shown in Figure 1 (top). For comparison, the model results without stratification are plotted on Figure 1 (bottom).

3.3. Previous Analysis of the SMILE Data

[19] The measurements have already been analyzed by *Santala* [1991], and part of its results were used by *Terray et al.* [2000] and RAT06. Here we will briefly summarize their analysis and the different method used here.

[20] Four velocity sensors were mounted on the SASS buoy, at depths from 1 to 5 m. The vertical shear can be estimated with the finite difference of velocities between pairs of adjacent sensors. *Santala* [1991] scaled the depth with u_*^2/g. This is equivalent to a significant wave height H_s scale, provided that swells are excluded in H_s and assuming that the wind sea is fully developed. The shear was scaled with u_*/z, the "law of the wall" scaling. These scalings yield their Figures 7–5, which we reproduce here for the SASS data only (Figure 2).

[21] The analysis of this plot, together with deeper measurements from a conventional mooring, lead these authors to propose a description of the downwind shear in a three-layer structure, namely an upper layer with almost no shear, a lower layer following a log-law, and a transition layer in between. However, such a transition is hardly perceptible with only the SASS data, because the lowest shear estimate falls in the transition region (Figure 2, left). In the crosswind direction, the shear was found roughly constant with depth. This analysis leads to Figures 7–11 in the work of *Santala* [1991], which was reproduced by *Terray et al.* [2000] and RAT06, showing the current profiles inferred from this analysis. These profiles were used afterward in the discussion of *Santala* [1991].

3.4. New Analysis of the SMILE Data

[22] It is not obvious from Figure 2 that the fit to the finite difference estimated shears produces a reliable value of the mean shear. Because of the wave-induced mixing, the near-surface vertical shear should better be scaled with u_*/H_s [*Craig and Banner*, 1994]. Even with this scaling, vertical profiles of the current shear remain quite noisy (Figure 3, circles).

[23] A more robust estimation of the mean vertical shear is given by a linear regression to the current measured at all 4 sensors. The choice of a linear profile corresponds to the constant near-surface shear expected in the wave-mixed

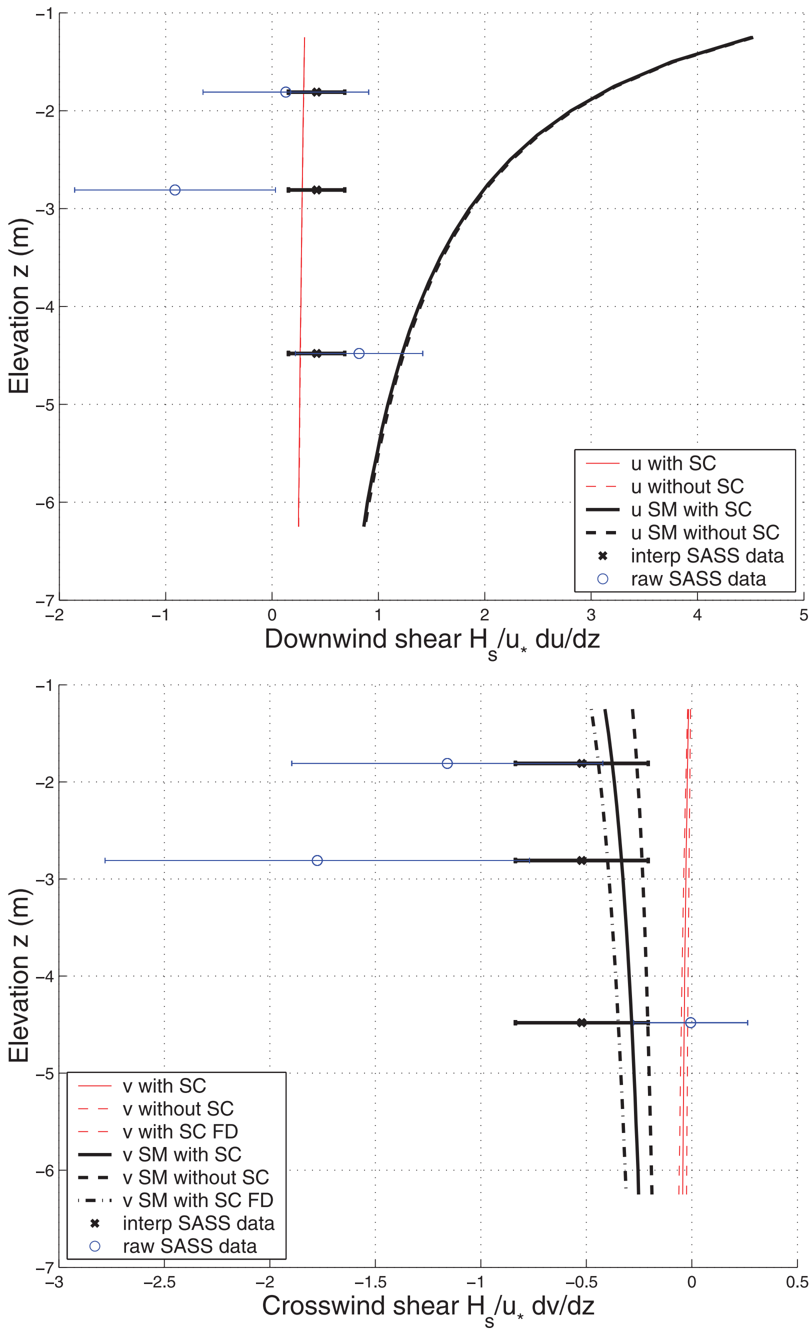

Figure 3. (top) Shear of the downwind component u of the current, normalized with u_*/H_s, plotted as function of the depth. Shears of the SASS data are calculated by finite difference between each pair of adjacent sensors. We show mean and standard deviation over the set of 13 records. The shears are calculated from the raw SASS data (circles) and from the SASS data linearly interpolated over the 4 current meter depths (crosses). Shears of the model are calculated by finite difference. In addition to the default model results, we plotted the results of the model without the Stokes-Coriolis effect (SC) and/or without the wave-induced surface mixing (SM, small mixing, obtained with a roughness length of z_0 = 0.05 m and no TKE surface flux). (bottom) Same as top but for the crosswind component v of the current. As an upper bound of the Stokes-Coriolis effect, the model results when supposing the wavefield fully developed (FD) are also shown.

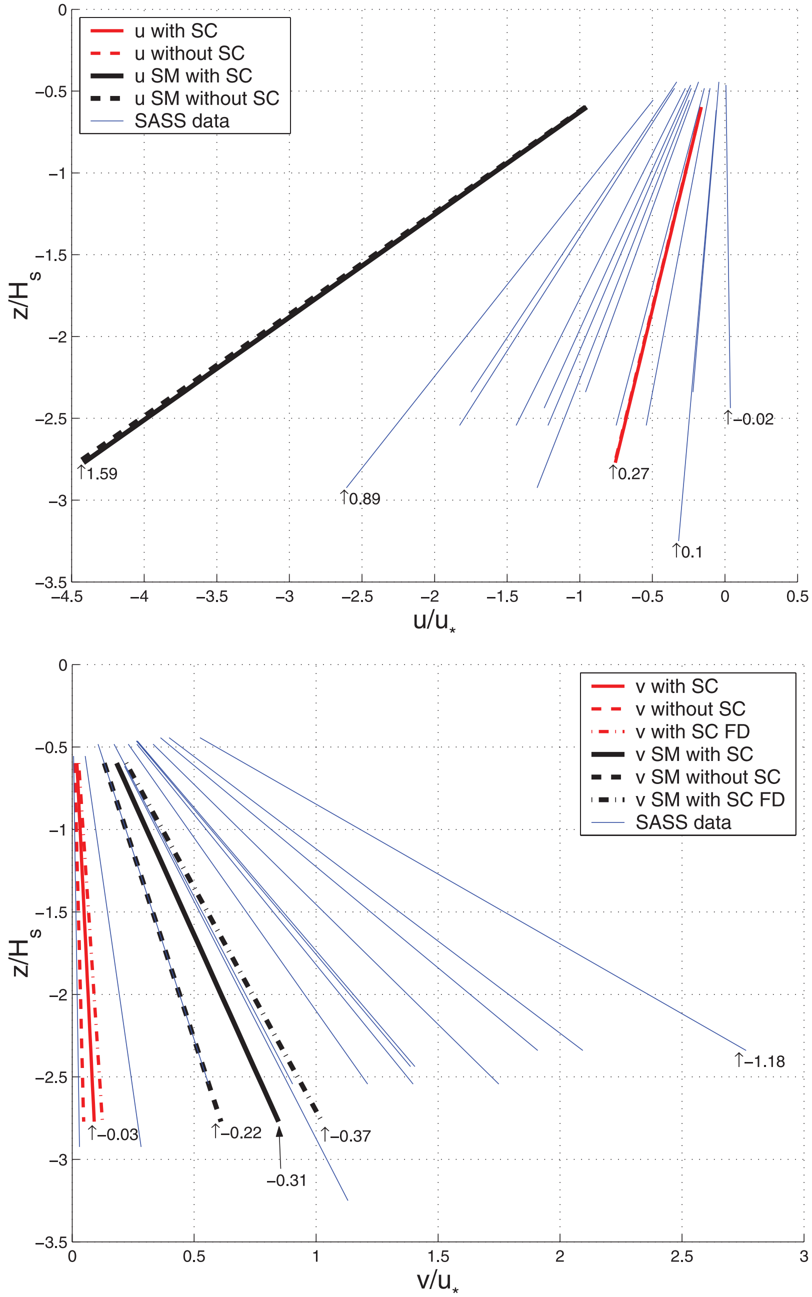

Figure 4. (top) Linear regression of the downwind current u between 1.1 and 5.8 m deep, the measurement depths of the SASS buoy. The current is normalized with u_* and the depth with H_s. The SASS data and different model results are plotted with an arbitrary offset. In addition to the default model results, we plotted the results of the model without the Stokes-Coriolis (SC) effect and/or without the wave-induced surface mixing (SM = small mixing, obtained with a roughness length of z_0 = 0.05 m and no TKE surface flux). (bottom) Same as top but for the crosswind component v. The SASS data are plotted, as well as different model results. FD, fully developed.

layer [*Craig and Banner*, 1994, equation (30)]. By imposing the vertical structure of the shear, this estimation method avoids the spreading due to finite difference shear estimations. It also reduces the scatter between the 13 records by a factor 3 to 4 (Figure 3).

[24] The observed and modeled shears are shown in Figure 4, with the elevation and current scaled by H_s and u_*, respectively. In the downwind direction (Figure 4, top) the observed shear, scaled by u_*/H_s, is 0.42 ± 0.26, where the first number is the mean and the second is the standard deviation. The corresponding downwind shear of the model is 0.27 with the full model. If the wave-enhanced near-surface mixing is omitted in the model (by using a small roughness length z_0 = 5 cm and by setting the TKE surface

flux to zero), the shear reaches 1.59. Although a linear fit is not a good approximation in this case, because the modeled current profile is close to logarithmic ("wall layer"), this analysis is consistent with our analysis of the observations. As was noted by *Terray et al.* [2000] and RAT06, the observations of quite weak near-surface downwind shears are consistent with an intense wave-induced mixing.

[25] In the crosswind direction (Figure 4, bottom) the mean nondimensional observed shear is -0.52 ± 0.31. The corresponding crosswind shear of the full model is -0.030, which is one order of magnitude smaller.

[26] The Stokes-Coriolis force, oriented in the crosswind direction, is a possible explanation for that large observed crosswind shear, because it is oriented to the right of the wave propagation, as is the observed shear bias. Therefore we made a quantitative evaluation of the Stokes-Coriolis impact on the crosswind current. Here, the wavefield is not fully developed and the Stokes transport is around 10% of the Ekman transport, which means that the Stokes-Coriolis effect is equivalent to a surface stress of 10% of the wind stress [*Polton et al.*, 2005]. The consequent crosswind shear (Figure 4, bottom) is quite small, increasing from -0.014 without the Stokes-Coriolis force to -0.030 with it. An upper bound for the Stokes-Coriolis stress can be found by supposing the wavefield fully developed. The equivalent stress is then 35% of the wind stress, but the crosswind shear only reaches -0.041 (Figure 4, bottom). The Stokes-Coriolis force is thus too weak to explain the large crosswind observed shears, and this is a consequence of the strong wave-induced mixing imposed in the model. Namely, if we omit the wave-induced mixing in the model, the crosswind shear reaches -0.22 without the Stokes-Coriolis force, -0.31 with it, and even -0.37 when supposing maximum value of the Stokes-Coriolis force, in better agreement with the observed shear. The SMILE observations of crosswind shear thus appear inconsistent with the wave-induced enhancement of the mixing, contrary to the downwind shear observations.

[27] Explanation for this asymmetry of crosswind and downwind shear observations might be found in anisotropic momentum transfer from wave breaking or in anisotropic wave-induced turbulence, in the presence of Langmuir circulations especially. The velocity profiles of different LES simulations of Langmuir turbulence [*McWilliams et al.*, 1997; *Noh et al.*, 2004] suggest that the mixing due to Langmuir cells is not isotropic. This is beyond the scope of the present numerical simulation.

[28] Also, if Langmuir circulations were present, the SASS buoy could have been trapped into surface convergence zones. *Santala* [1991] investigated the vertical velocity records and did find a nonzero mean downward velocity, interpreted as evidence of a nonuniform sampling of the Langmuir cells. The consequent bias on the horizontal velocity measurement cannot be excluded to explain the large observed crosswind shear.

4. Analysis of the Current Magnitude: LOTUS Data

[29] The impact of the Stokes-Coriolis effect and of the stratification is small on the current shear, but is more apparent on the magnitude of the current: the Ekman transport is trapped in the mixed layer, leading to large values of the crosswind current, while the Stokes-Coriolis effect gives small values, if not negative, of the downwind current (see, e.g., Figure 1, top). Are the observed current in agreement with that expected shape?

[30] Field measurements of the Ekman currents are always noisy, due to inertial oscillations and various other phenomena, some of them being surface-trapped. It is thus difficult to separate other processes from the mean wind-driven current. During SMILE (previous section), the currents were averaged over 40 mn. This allows an analysis of the vertical shears but it is insufficient to investigate the magnitude of the current. One solution to get rid of this noise is to average the current over a long time period. This method has been employed by *Price et al.* [1987] with the LOTUS 3 [*Tarbell et al.*, 1984] data set.

[31] The LOTUS 3 experiment took place in the western Sargasso Sea (34°N, 70°W) in the summer of 1982, under light to moderate winds, $U_{10} = 5.4 \pm 2.7$ m s^{-1}, and strong diurnal heating, with an average of the daily maximum net surface heat flux of 630 W m^{-2} [*Price and Sundermeyer*, 1999]. The current measurements came from Vector Measuring Current Meters (VMCMs) along a conventional mooring, with the upper measurements at 5-, 10-, 15-, and 25-m depth. In the typical light wind encountered, waves were small, $H_s = 1.3 \pm 0.7$ m, so that the wave-induced bias, i.e., the correlation between the motion of the mooring and the orbital motion of the waves, was first estimated to be small at the measurement depths using VMCMs [*Schudlich and Price*, 1998]. We will further discuss this point below. Finally *Price et al.* [1987] used a coherent averaging method to follow the low-frequency changes in wind direction. The resulting current profile can then be quantitatively compared to theoretical models of the Ekman current. This observed current has the expected profile of an Ekman spiral, with a depth integrated transport in agreement with the Ekman transport. However, some features were unexpected. First, the subsurface deflection is quite large, around 75° at a depth of 5 m. Second, the decay with depth is stronger than the clockwise rotation (the spiral is "flat").

[32] To explain this flatness of the spiral, *Price and Sundermeyer* [1999] invoked the temporal variation of stratification. The mixed layer depth varied typically from 10 m during the day to 25 m at night. The mean current, time averaged over the diurnal cycle, is thus rectified, and exhibits a different vertical profile than the current inferred from the mean vertical stratification [see also *McWilliams and Huckle*, 2006].

[33] Later, *Lewis and Belcher* [2004] and *Polton et al.* [2005] noted that the approach of *Price and Sundermeyer* [1999] is not able to reconcile the observed large subsurface deflection of 75° and a small surface deflection of 10 to 45° typically observed from drifting objects [*Huang*, 1979]. Ignoring the stratification, *Lewis and Belcher* [2004] and *Polton et al.* [2005] argued that the Stokes-Coriolis force can explain the large subsurface deflection, together with a small surface deflection. The agreement between their models and the LOTUS 3 observations was then quite good [see *Polton et al.*, 2005, their Figure 8].

[34] Other problems appear in turn in these models. First, the small surface deflections reviewed by *Huang* [1979]

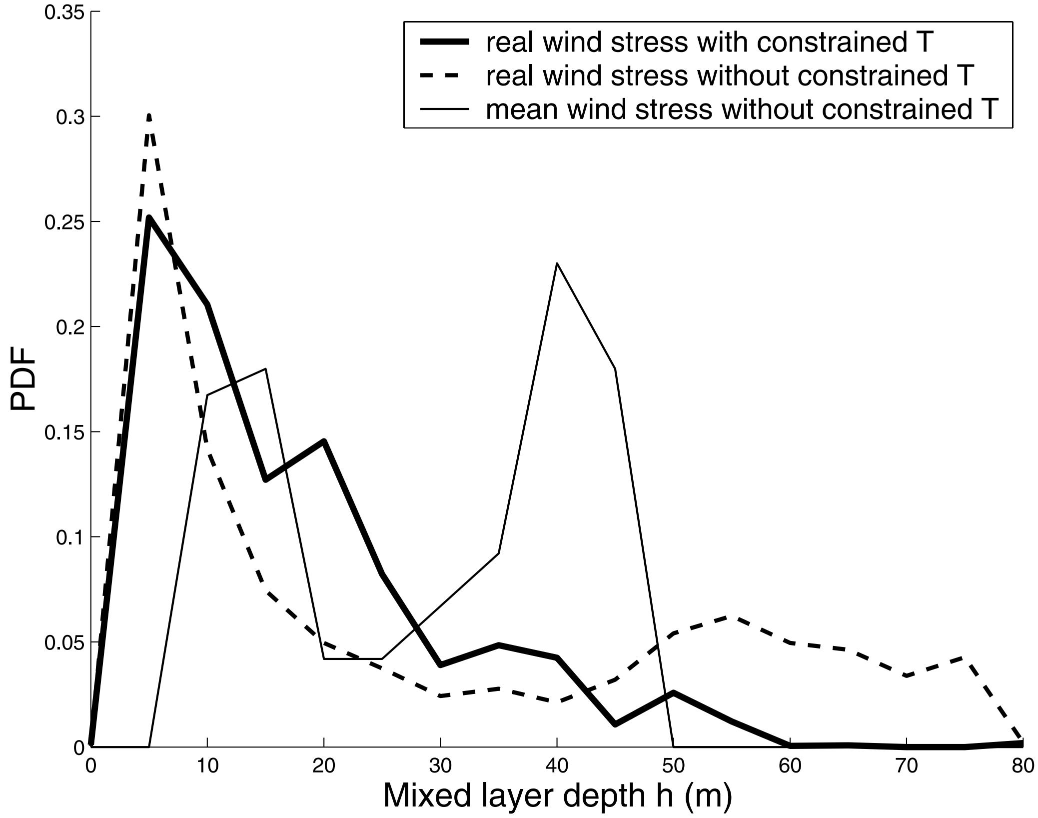

Figure 5. Probability density functions of the hourly mixed layer depth of three numerical simulations of the LOTUS 3 measurement. The mixed layer depth is defined with a criterion on attenuation of surface TKE [*Noh*, 2004]. All model runs use the analytical heat flux (15), which closes the heat budget. Thin solid line is the model with the mean observed wind stress (section 4.1), dashed line is with the observed variable wind (section 4.2), and thick solid line is with the observed wind and with the temperature assimilation (section 4.3). T, temperature.

mainly come from observations of Lagrangian surface drift. As noted by RAT06, the Lagrangian surface drift is the sum of the Stokes drift and the quasi-Eulerian current. A large surface deflection of the quasi-Eulerian current is not contrary to a small surface deflection of the Lagrangian drift, because of the Stokes drift. In relation to this, the surface mixing in the models of *Lewis and Belcher* [2004] and *Polton et al.* [2005] is likely to be several orders of magnitude too small. But, as noted by RAT06 without stratification, a realistic surface mixing gives a quasi-Eulerian current much more uniform than modeled by the previous authors, ruining the agreement with the data (see the work of RAT06, Figure 7). Stratification is therefore needed to reexamine the LOTUS 3 data. Here we also reexamine whether or not the LOTUS 3 data offer an observational evidence of the Stokes-Coriolis effect on the Ekman current.

4.1. Simple Model of the Diurnal Cycle

[35] Following the idealized model of *Price and Sundermeyer* [1999], the present model is run with the mean wind stress observed during the period, $u_* = 0.0083$ m s^{-1}. The waves are expected to be fully developed with that wind stress, which gives a significant wave height of $H_s = 1.6$ m, based on the spectrum of *Kudryavtsev et al.* [1999].

[36] The temperature is initialized with the temperature observed at the beginning of the field experiment. For the surface heat flux, we use an analytical fit of the solar insolation measured during clear sky days and we suppose that a steady heat loss equilibrates the surface heat budget,

$$Q = \max\left(0, 1000\cos\left(\frac{2\pi t}{T_{day}}\right)\right) - \frac{1000}{\pi}, \qquad (15)$$

where t is the time and T_{day} is a period of one day.

[37] The mixed layer depth h is calculated using the model criteria $E(h) < E(z = 0) \times 10^{-4}$. The probability density function (PDF) of the mixed layer depth is shown in Figure 5, showing a bimodal distribution corresponding to diurnal and nocturnal mixed layers. With these mean wind stress, surface heat flux, and initial temperature, the mixed layer depth varies between 8 m and 40 m, as observed during LOTUS 3 (Figure 5). However the vertical profile of the current is very different from the observed one. The modeled current is too large and homogeneous within the mixed layer (Figure 6).

[38] Not surprisingly, the velocity profile is not well reproduced when we use the mean wind stress. The rectification over subperiods with weak wind should not leave a mean velocity profile homogeneous in the upper 8 m.

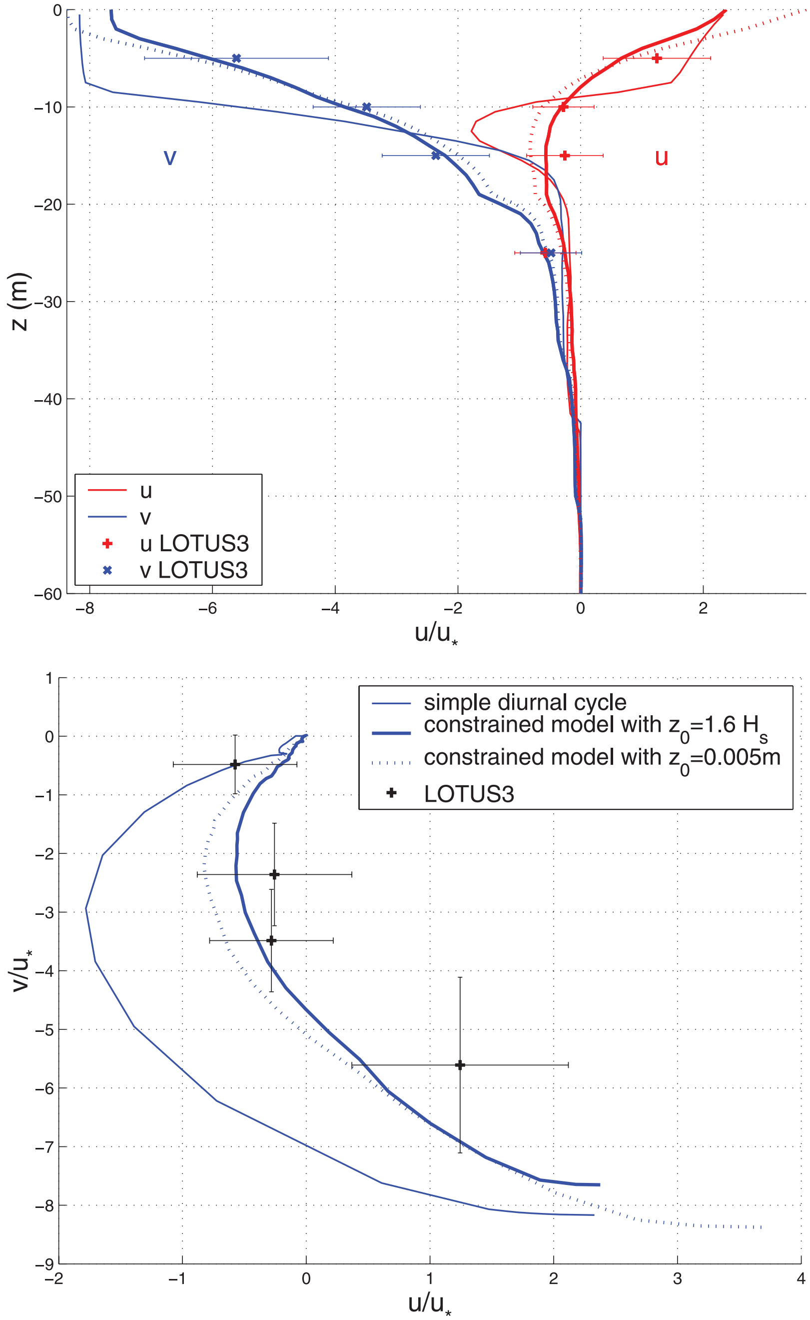

Figure 6. Mean currents obtained in three different LOTUS 3 simulations, each without the Stokes-Coriolis force. (top) Vertical profiles of the mean current $(\widehat{u}, \widehat{v})$. (bottom) Hodographs of the mean current. Each simulation uses the analytical heat flux (15). Thin line uses the mean wind stress (section 4.1). Thick solid and dotted lines use the variable wind stress and the constrained temperature (section 4.3) and test the sensitivity to the wave-induced mixing with roughness lengths $z_0 = 1.6\ H_s$ and $z_0 = 0.005$ m, respectively. The LOTUS 3 data are plotted together with their standard errors, calculated from a statistical analysis by *Schudlich and Price* [1998, Table 1].

Similarly, if a strong wind event occurred during the measurement period, its effect must be apparent on the mean velocity profile below 30 m deep.

4.2. More Elaborate Model: Using the Wind History

[39] The previous results using the average wind stress are encouraging but the profile of the mean current exhibits a large sensitivity to the mixed layer depth history. The temperature variability is not well reproduced with only a simple reproduction of the diurnal cycle. We will therefore attempt a more realistic simulation of the LOTUS 3 data, using the full recorded history of the wind stress.

[40] For computational simplicity, the wind direction is taken constant, in agreement with the coherent averaging of *Price et al.* [1987]. This simplification can be further justified by the absence of any clear indication of what

the damping of inertial oscillations should be in a one dimensional model [e.g., *Mellor*, 2001]. The bulk formulation of COAMPS [*Hodur et al.*, 2002] for the atmospheric boundary layer is used to calculate the wind stress. The relative humidity is set to 75%, as in the work of *Stramma et al.* [1986]. The wind stress is 6 hr low-pass-filtered. Using the filtered wind stress and not the filtered wind speed conserves the stress and minimizes the rectification errors. Finally, the current of the model, averaged over 1 hr, is stored and used to calculate the mean over the whole time period (170 days).

[41] When one wants to reproduce the stratification, both the heat budget and the large-scale advection of heat come into play. Attempting to validate their 1D model of the ocean vertical mixing, *Gaspar et al.* [1990] analyzed a 2 weeks subset of the LOTUS 3 measurements. They reported imbalance of the order of 80 W m^{-2} in the ocean heat budget. They estimated large-scale advection to be responsible for an imbalance of 15 W m^{-2}. Remaining errors were attributed to the bulk derived heat fluxes and uncertain estimations of latent heat flux [see *Stramma et al.*, 1986] and of solar infrared flux, due to missing measurements of relative humidity and of cloud type, respectively.

[42] These uncertainties on the advection and heat flux are critical for a simulation of the observed temperature, as the model temperature might slowly drift away from observations. However, the present study investigates currents, for which the mixed layer depth is more important than the absolute value of the temperature. The analytical heat flux (15) and the observed wind stress may suffice to produce an adequate mixed layer history. During day time the model yields good results (Figure 5, see the agreement between dashed and thick solid lines for mixed layers less than 10 m), as the thickness of the diurnal mixed layer is determined by the Monin-Obukhov length scale, i.e., by the surface heat and momentum fluxes. However, the nocturnal convection and its effect on stratification are also determined by the temperature profile and the water column heat content, especially when the nocturnal heat loss exceeds the preceding diurnal heat gain. The analytical heat flux (15) leads to a small negative drift of the model temperature, and thus to large overestimations of nocturnal mixed layer depth (Figure 5, see the discrepancies between dashed and thick solid lines for mixed layers deeper than 50 m).

4.3. Pragmatic Model: Constraining the Stratification

[43] In order to avoid errors due to differences in stratification, we will constrain the temperature to the observed temperature. Every 6 hr, we reinitialize the temperature of the model to the 1-hr mean observed temperature. The analytical fit (15) for the heat flux is still used to reproduce the high-frequency diurnal cycle. The temperature of the simulation is therefore in close agreement with the observed temperature (correlation coefficient above 0.99 at every measurement depth), including the diurnal stratification, except during a few episodes of exceptionally weak solar insolation not captured with our simple heat flux (15).

4.4. Model Results

[44] The modeled current averaged over the entire period and the coherent averaging of observations by *Price and Sundermeyer* [1999] are shown in Figures 6 and 7. The crosswind current agrees well with the observations, with differences less than 0.36 cm s^{-1} (= 0.45 u_*) and relative errors of less than 10% for the 3 upper measurements. The crosswind transport of the model is equal to the Ekman transport, corresponding to the mean wind stress, while the crosswind transport calculated with a trapezoidal extension of the data is slightly (8%) inferior [see also *Price et al.*, 1987]. The downwind current of the model, if we omit the Stokes-Coriolis effect, is in correct agreement with the observations, with differences less than 0.47 cm s^{-1} (= 0.58 u_*) which still represent relative errors of the order of 100%. The downwind transport of the model without the Stokes-Coriolis effect is nil, and the downwind transport from the extrapolated data is around -1.9×10^{-3} m^2 s^{-1}, which is 0.26% of the crosswind Ekman transport.

[45] Such agreement between the model and the observations is encouraging. It provides the opportunity to estimate the importance of the different ingredients of the model. In particular, we test the model sensitivity to the roughness length. As shown in Figure 6, the mean velocity profile is mainly determined by the stratification and the consequent rectification effect. The wave-induced mixing is less discernable on velocity measurements below 5-m depth than above, and at those depths it is hard to discriminate between small and large values of the roughness length.

4.5. Stokes-Coriolis Effect

[46] The Stokes drift has been calculated by supposing the wavefield fully developed with the corresponding wind averaged over 6 hr. This gives an upper bound of the Stokes-Coriolis effect (Figure 7, dotted line).

[47] A more realistic estimation of that effect is also needed. The complete historic of the waves during the period is preferable, because it includes possible correlations between large wave events, strong wind events, and particular stratification events like deep mixed layers. Therefore a global wave model of 1° resolution is used to produce the sea state at the LOTUS 3 station (34.0N, 70.0W). The wave model is based on the WAVEWATCH III (WW3) code [*Tolman et al.*, 2002], in which the wind wave evolution parameterizations have been replaced by those of *Bidlot et al.* [2005]. Although these parameterizations still have some problems in coastal and swell-dominated areas [*Ardhuin et al.*, 2007], they provide good results for the mean parameters H_s and T_{m02} when compared to the North Atlantic buoys measurements [*Ardhuin and Le Boyer*, 2006; *Rascle et al.*, 2008; *Bidlot et al.*, 2007]. This model is forced with 10-m winds 6-hourly ERA 40 reanalysis [*Uppala et al.*, 2005] from the European Center for Medium-Range Weather Forecasting (ECMWF). The comparison with the nearby buoy 41001 (34.7N, 72.7W) of the National Data Buoy Center (NDBC) shows an RMS error of 0.43 m on H_s (25% of the RMS H_s) and of 0.57 s on the mean period T_{m02} (9.8% of the RMS T_{m02}), for the period from 14 May to 30 November 1982. Note that no wave data were available at that buoy from 6 June to 6 August. Our calculation might underestimate the Stokes transport since there is a significant negative bias on the wave height H_s (-0.25 m), and a negligible bias on the mean period T_{m02} (-0.07 s).

[48] The wave spectra at the LOTUS 3 station were used to compute the Stokes drift. Consistent with the averaging

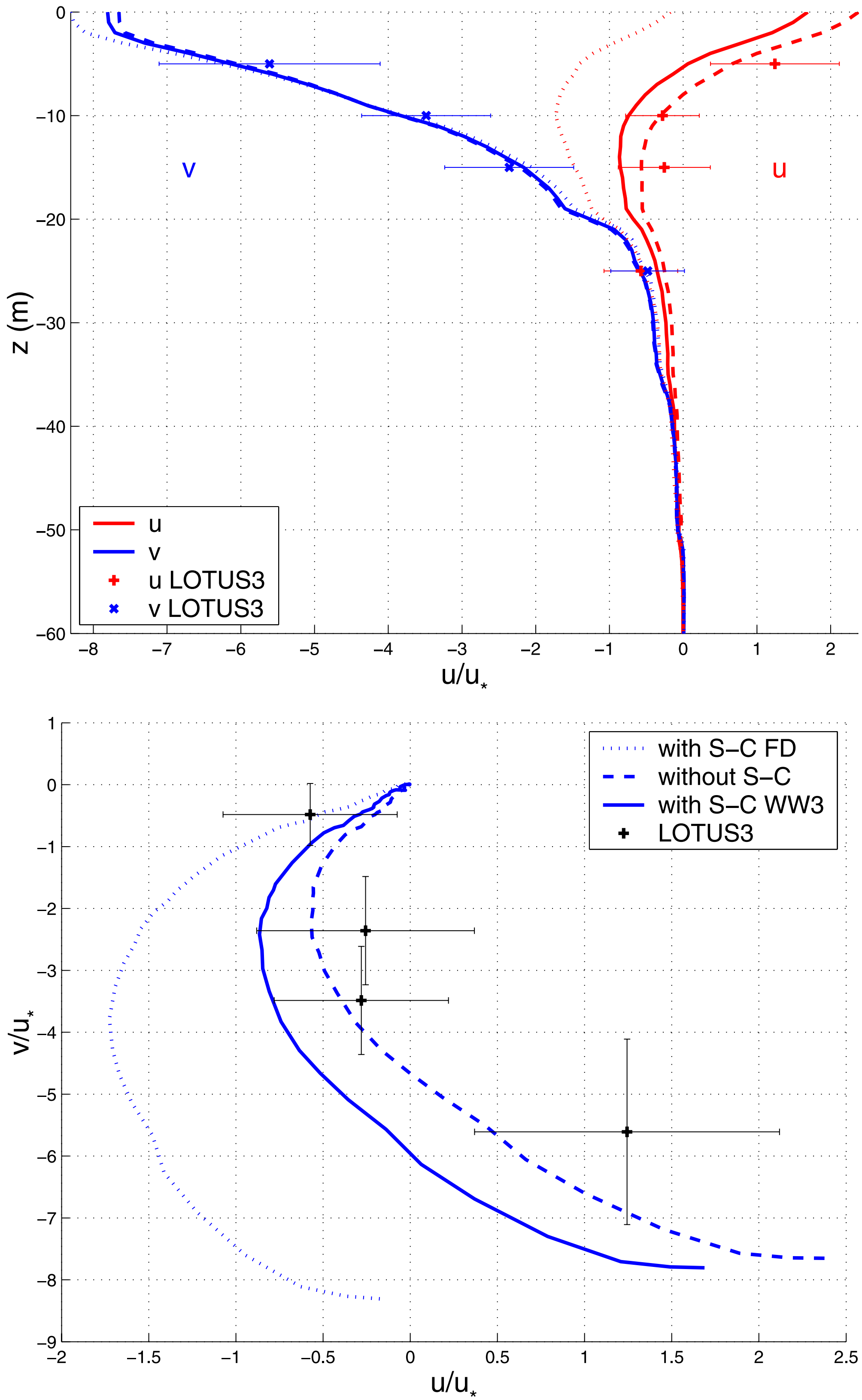

Figure 7. LOTUS 3 simulation, using the observed wind stress and with the temperature constrained to the data. (top) Vertical profiles of the mean current ($\widehat{u}$, $\widehat{v}$). (bottom) Hodographs of the mean current. Dashed lines are the model results without the Stokes-Coriolis effect. Dotted lines are the model results when supposing the waves fully developed (with the 6-hr low-pass-filtered wind), giving an upper bound of the Stokes-Coriolis effect. Solid lines represent model results, with the Stokes-Coriolis effect calculated using the WW3 wave hindcast. FD, fully developed.

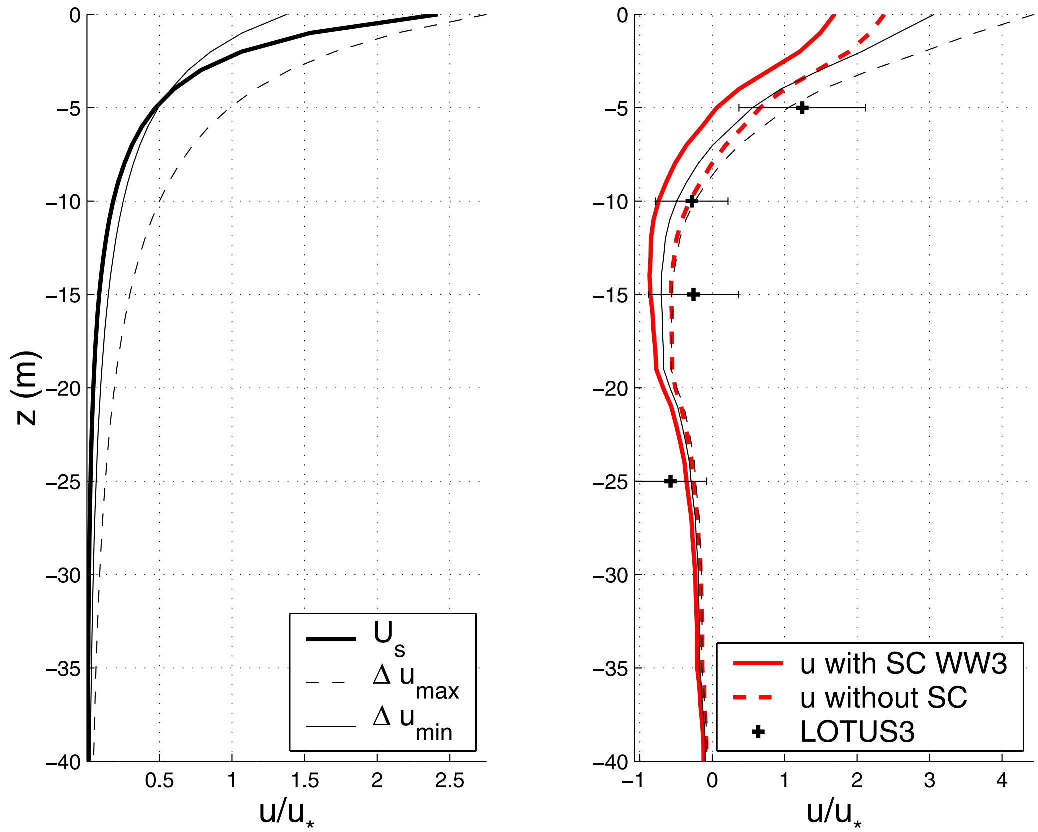

Figure 8. Wave-induced bias on the LOTUS 3 measurements. (left) Vertical profiles of the averaged norm of the Stokes drift $\mathbf{U}_s$ (thick solid line), Δu_{max} (thin dashed line), and Δu_{min} (thin solid line). (right) Profile of velocity $\widehat{u}$ calculated with the Stokes-Coriolis effect from the wave reanalysis (thick solid line, similar to Figure 7), augmented with the additional bias Δu_{min} (thin solid line) and Δu_{max} (thin dashed line). Also shown is the velocity $\widehat{u}$ calculated without the Stokes-Coriolis effect (thick dashed line, similar to Figure 7).

method of *Price et al.* [1987], we rotate the Stokes drift components following the wind direction. To avoid any discrepancy between the observed and reanalyzed wind direction, we need to use the ERA 40 wind direction. For computational simplicity, we use the surface Stokes drift direction as a proxy for the ERA 40 wind direction. This approximation is reasonable because at the surface, the Stokes drift is a high moment of the spectrum, and it is closely aligned with the wind. In support of this approximation, we found the average of the Stokes drift (rotated following the wind) over the whole time period to be aligned with the wind. The mean crosswind Stokes transport is only 2.3% of the downwind Stokes transport. This means the mean contribution of waves not aligned with the wind (i.e., swell) is weak. For additional simplicity, we use the norm of the Stokes drift and prescribe it to be aligned with the wind at each depth at every time step. This second simplification leads to an increase of the mean downwind Stokes transport by 2.6%, which is negligible compared to the uncertainties of the wave reanalysis.

[49] The numerical results with that estimation of the Stokes-Coriolis term are shown in Figure 7. The mean Stokes transport is 0.075 $m^2\ s^{-1}$, i.e., 9.5% of the Ekman transport which reaches 0.79 $m^2\ s^{-1}$. Accordingly, the mean downwind current transport of the model with the Stokes-Coriolis effect is $-0.091\ m^2\ s^{-1}$, which compensates the Stokes transport (within a 17% error which may be due to insufficient vertical dicretization or rectification). On the contrary the downwind transport from the extrapolated data is almost nil ($-1.9 \times 10^{-3}\ m^2\ s^{-1}$).

[50] Similarly, the downwind current profile of the model is closer to the data when we omit the Stokes-Coriolis term (Figure 7). In this regard, the present work is consistent with the work of *Price and Sundermeyer* [1999], showing that the "flatness" of the spiral results from the stratification, in contradiction to *Polton et al.* [2005], who claimed that it is due to the Stokes-Coriolis effect.

4.6. Wave-Induced Bias

[51] One explanation emerges for that apparent misfit of the model when including the Stokes-Coriolis effect: the observed downwave velocities were supposed to be Eulerian but could have been contaminated by the wave-induced buoy motion. Namely, the mooring line measured 5395 m in 5366 m of water and was thus almost vertical. One can then consider that the subsurface current meter motion follows the surface buoy motion, and this should yield a wave-induced bias due to correlations between orbital wave motion and current meter motion [*Pollard*, 1973]. *Schudlich and Price* [1998] used the method of *Santala* [1991] to discuss this wave-induced bias. In particular, one can

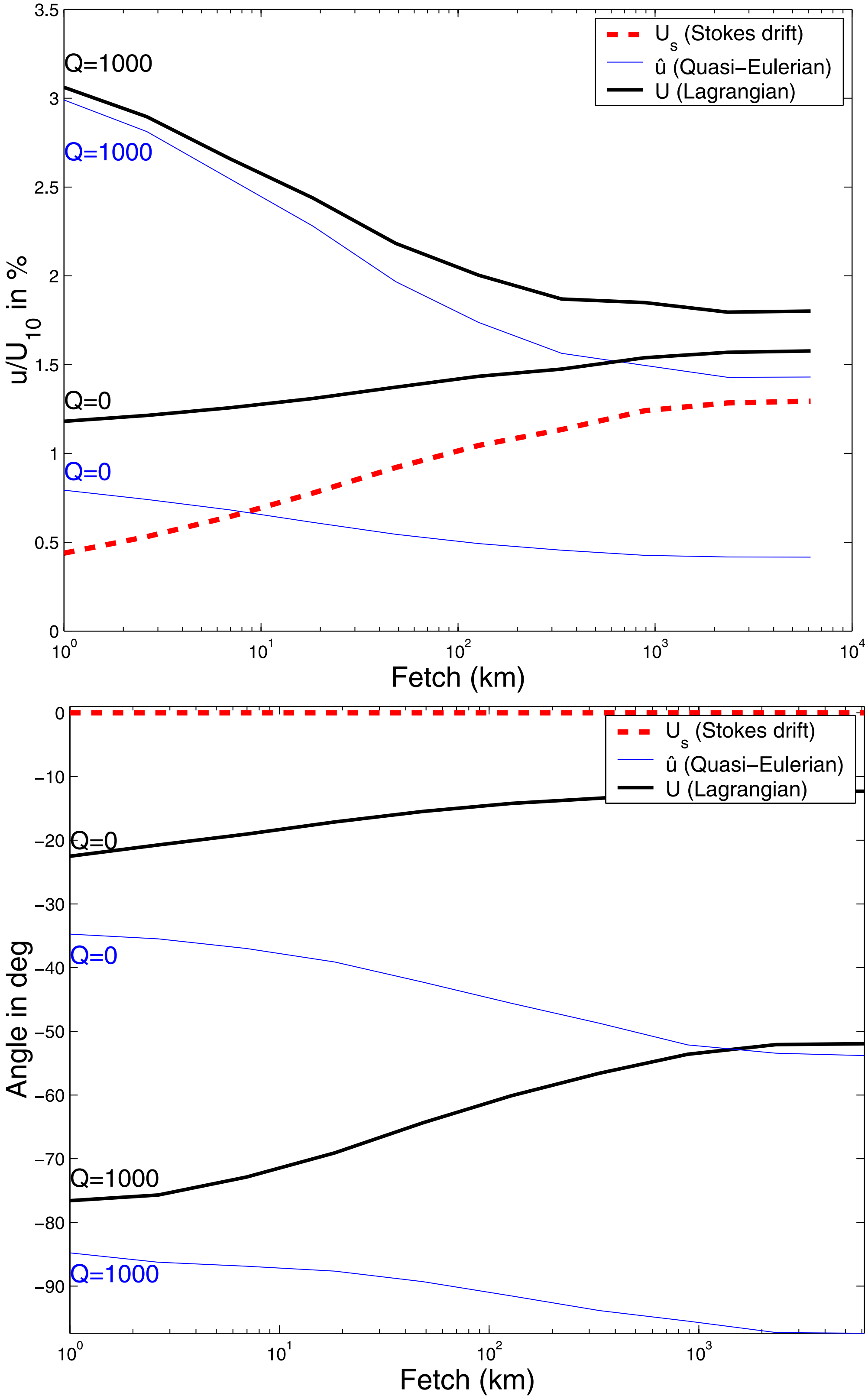

Figure 9. (top) Stokes drift $\mathbf{U}_s$, quasi-Eulerian current $|\widehat{\mathbf{u}}|$, and total Lagrangian drift $\mathbf{U} = |\widehat{\mathbf{u}} + \mathbf{U}_s|$ at the surface ($z = -0.5$ m) as function of fetch. The velocities are expressed as a percentage of the wind speed U_{10}. The wind is set to $U_{10} = 10$ m s^{-1}, and two different stratifications are obtained from an initially uniform density and applying two different surface heat fluxes, $Q_h = 0$ and 1000 W m^{-2}. The Stokes drift is calculated from the spectrum of *Kudryavtsev et al.* [1999]. (bottom) Corresponding angles of deviations from the wind direction, measured counterclockwise.

suppose that the buoy moves vertically with the surface. Then, for each monochromatic wave train, one gets in addition to the quasi-Eulerian current a bias equal to

$$\Delta u_{\min}(z) = \frac{1}{2} a^2 \omega k \exp(-kz), \tag{16}$$

where z is the elevation measured downward, a is the wave amplitude, ω is the radian frequency, and k the wave number. This estimation gives a lower bound of the wave-induced bias. Assuming that the buoy moves both vertically and horizontally, the maximum wave-induced bias is

$$\Delta u_{\max}(z) = a^2 \omega k \exp(-kz). \tag{17}$$

For comparison, the Stokes drift of a monochromatic wave is

$$U_s(z) = a^2 \omega k \exp(-2kz). \tag{18}$$

As the wave-induced motions of the current meters are larger than the wave-induced motions of the particles, the maximum bias is larger than the Stokes drift (the equality arises at the surface only [see Figure 8, left]).

[52] The wave spectrum predicted by the wave model gives the average over the whole LOTUS 3 period of $\Delta u_{\min}$ and $\Delta u_{\max}$ (Figure 8, left). Those biases have also been added to the downwind current of the model with the Stokes-Coriolis effect (Figure 8, right, thin lines).

[53] The vertical integral of the bias is bounded by

$$M^w \leq \int_{-H}^{0} \Delta u dz \leq 2M^w, \tag{19}$$

where M^w is the Stokes transport ($= a^2\omega/2$ for a monochromatic wave). Therefore, as the theoretical downwind transport is equal to $-M^w$, the biased transport is composed of between 0 and $+M^w$ (Figure 8, right, thin lines). The observed downwind transport in LOTUS 3 is approximately zero. It was interpreted by *Price et al.* [1987] as an evidence that the Ekman transport is crosswind. However, the downwind transport induced by the Stokes-Coriolis effect is not negligible (equal in magnitude to the Stokes transport, which reaches 9.5% of the Ekman transport) and should have been observed. We argue here that it was not observed because of the wave-induced bias. Furthermore, in the winter measurements of LOTUS 4, a positive downwind transport was found and was interpreted by *Schudlich and Price* [1998] as a wave-induced bias, coming from the large winter waves. The present description supports the more nuanced conclusion that both the LOTUS 3 and the LOTUS 4 measurements are likely biased by the waves in the downwind direction.

5. Surface Drift

[54] One aim of the present model is a better understanding of the surface Lagrangian drift, for applications to search and rescue, fish larvae recruitment, or any other studies following floating materials. The present model, following *Garrett* [1976] and *Jenkins* [1989], separates the flow into a wave Stokes drift and a quasi-Eulerian current. In particular, the introduction of the wave age should bring new insight in the near-surface dynamics. One remarkable result obtained by RAT06 for unstratified conditions is that the surface drift is almost independent of the wave age: in one hand, as the waves get more mature, the Stokes drift increases. However, in the other hand, the mixing also gets more efficient and leaves an Ekman current more homogeneous, thus reducing the surface quasi-Eulerian current. Therefore the surface drift, which is the sum of the Stokes drift and of the quasi-Eulerian current, does not vary much with the wave age. This result is recalled in Figure 9 (top, for $Q_\mathrm{h} = 0$ W m^{-2}; note that the quasi-Eulerian current is weaker at the surface compared to results obtained in the work of RAT06 (Figure 12) due to the poorer vertical resolution, the first level being at -0.5 m in the present model).

[55] Whereas the wave age is a key parameter for the near-surface mixing, it has little influence on the surface drift in unstratified conditions. A simple parameterization of the surface drift directly from the wind might then be possible. However, this result does not hold in stratified conditions.

[56] The dependance of the surface drift on the wave age in the presence of strong stabilizing buoyancy flux (Q_h = 1000 W m^{-2}, which gives a Monin-Obukhov length scale L = 2.8 m) is shown in Figure 9. For strong buoyancy forcing, the mixed layer is shallow (around 8–12 m) so that the quasi-Eulerian surface current is almost crosswind (angle around $-90°$). Due to this large deviation angle, increase of the Stokes drift cannot compensate reduction of the quasi-Eulerian current, when waves get more developed and mixing more efficient. The surface drift is thus a decreasing function of the wave age (see Figure 9, top, for Q_h = 1000 W m^{-2}), contrary to what happens in unstratified conditions where the angle between the Stokes drift and the quasi-Eulerian current is more modest (angle around 45° [see Figure 9, bottom]). In addition, the mixed layer of the model gets thicker with a larger wave-induced mixing (from 8 m for short fetches to 12 m for large fetches), which further increases the wave age dependance of the surface drift during strong heating events. The surface drift thus reaches 3% of the wind speed U_{10} for very shallow mixed layer associate with small fetches. That mixed layer depth dependency on the wave age is physically sound but requires further verifications. Useful validation data were acquired during the C-BLAST experiment off the U.S. east coast and are still being processed (T. P. Stanton, Naval Postgraduate School, Monterey, CA, personal communication).

6. Conclusion

[57] A model of the surface layer of the ocean was presented by RAT06. Essentially, the current was separated into a wave Stokes drift and a quasi-Eulerian current. That physical description led to a different analysis of the observations of currents profiles close to the surface, whether the measurements are Eulerian or Lagrangian. That analysis agreed qualitatively with a few available data of Lagrangian drift profiles, of Eulerian velocity profiles, and of TKE dissipation rates. Motivated by these results, this

work is extended here by including the stratification, allowing a more quantitative validation of the current profiles.

[58] We performed a reanalysis of the near-surface quasi-Eulerian velocity measurements during SMILE. The near-surface shears were previously investigated under the hypothesis of a three-layer structure [*Santala*, 1991]. Here we made no hypothesis on the structure of the shear and we linearly interpolate the upper current measurements. The near-surface shears obtained are found to be in good agreement with the downwind shears expected in the presence of a strong wave-induced mixing. However, crosswind shears found are an order of magnitude larger than expected. These large crosswind shears cannot be explained by the Stokes-Coriolis force, which is one order of magnitude too weak. Models and complementary observations of Langmuir cells appear therefore to be necessary for further investigations of these near-surface current measurements.

[59] The long-term observations of Ekman spirals during LOTUS 3 provide an opportunity to investigate the Stokes-Coriolis effect. The use of a long time series reduces the noise in the measurement, enabling an analysis of the magnitude of the wind-driven current. However, it introduces rectification effects because of the temporal variations of the wind and of the stratification. The wind variability is taken into account by using the coherent averaging of *Price et al.* [1987], which follows the wind direction, and changes in the stratification are represented by constraining the temperature to the observed temperature. The Ekman spiral of the model then shows good agreement with the observations. However, we do not find any evidence of the Stokes-Coriolis effect, whereas accurate wave hindcasts suggest that it should be significant, leading to upwind transport around 10% of the crosswind Ekman transport. Beside errors coming from the large variability of the instantaneous current, the nature of the measurement might be in question, because the bias induced by the waves on near-surface measurements from a buoy can be larger than the Stokes transport. Seeking evidence of the Stokes-Coriolis effect in such long time averaging, as attempted by *Lewis and Belcher* [2004] and *Polton et al.* [2005], still appears to be feasible but preference should be accorded to measurements from fixed towers to get rid of that wave-induced bias.

[60] Finally, we investigated the surface drift predictions of the model in the presence of stratification. It is shown that the wave age effect on the surface drift, which was found to be small in unstratified conditions, is important in the presence of shallow diurnal mixed layers. In such case, considering separately the wavefield and the mean current should give significant differences on surface drift predictions.

[61] **Acknowledgments.** The initial version of the computer code for the mixed layer model was kindly provided by Yign Noh. We acknowledge the National Buoy Data Center (NDBC) and the Upper Ocean Mooring Data Archive of the Woods Hole Oceanographic Institution (WHOI) for their Web-available data. We also thank the careful anonymous reviewer who yielded a significant improvement of the manuscript. N.R. acknowledges the support of a CNRS-DGA doctoral research grant.

References

Agrawal, Y. C., E. A. Terray, M. A. Donelan, P. A. Hwang, A. J. Williams, W. Drennan, K. Kahma, and S. Kitaigorodskii (1992), Enhanced dissipation of kinetic energy beneath breaking waves, *Nature*, *359*, 219–220.

Andrews, D. G., and M. E. McIntyre (1978), An exact theory of nonlinear waves on a Lagrangian-mean flow, *J. Fluid Mech.*, *89*, 609–646.

Ardhuin, F., and A. Le Boyer (2006), Numerical modelling of sea states: Validation of spectral shapes (in French), *Navigation*, *54*(216), 55–71.

Ardhuin, F., T. H. C. Herbers, K. P. Watts, G. P. van Vledder, R. Jensen, and H. Graber (2007), Swell and slanting fetch effects on wind wave growth, *J. Phys. Oceanogr.*, *37*(4), 908–931, doi:10.1175/JPO3039.1.

Ardhuin, F., N. Rascle, and K. A. Belibassakis (2008), Explicit wave-averaged primitive equations using a generalized Lagrangian mean, *Ocean Modell.*, *20*, 35–60, doi:10.1016/j.ocemod.2007.07.001.

Beardsley, R. C., E. P. Dever, S. J. Lentz, and J. P. Dean (1998), Surface heat flux variability over the northern California shelf, *J. Geophys. Res.*, *103*, 21,553–21,586.

Bidlot, J., S. Abdalla, and P. Janssen (2005), A revised formulation for ocean wave dissipation in CY25R1, *Tech. Rep. Memo. R60.9/JB/0516*, Res. Dep., ECMWF, Reading, U. K.

Bidlot, J. R., et al. (2007), Inter-comparison of operational wave forecasting systems, in *Proceedings of the 10th Int. Workshop on Wave Hindcasting and Forecasting and Coastal Hazard, U.S. Army Eng. Res. and Dev. Center's Coastal and Hydraulics Lab.*, North Shore, Oahu, Hawaii, 11–16 Nov.

Charnock, H. (1955), Wind stress on a water surface, *Q. J. R. Meteorol. Soc.*, *81*, 639–640.

Craig, P. D., and M. L. Banner (1994), Modeling wave-enhanced turbulence in the ocean surface layer, *J. Phys. Oceanogr.*, *24*, 2546–2559.

Ekman, V. W. (1905), On the influence of the earth's rotation on ocean currents, *Ark. Mat. Astron. Fys.*, *2*, 1–53.

Garrett, C. (1976), Generation of Langmuir circulations by surface waves—A feedback mechanism, *J. Mar. Res.*, *34*, 117–130.

Gaspar, J. P., Y. Grégoris, and J. M. Lefevre (1990), A simple eddy kinetic energy model for simulations of oceanic vertical mixing: Tests at station papa and long-term upper ocean study site, *J. Geophys. Res.*, *95*, 16,179–16,193.

Hasselmann, K. (1970), Wave-driven inertial oscillations, *Geophys. Fluid Dyn.*, *1*, 463–502.

Hasselmann, K., et al. (1973), Measurements of wind-wave growth and swell decay during the Joint North Sea Wave Project, *Dtsch. Hydrogr. Z.*, *8, suppl. A*(12), 1–95.

Hodur, R. M., J. Pullen, J. Cummings, X. Hong, J. D. Douyle, P. J. Martin, and M. A. Rennick (2002), The Coupled Ocean/Atmosphere Mesoscale Prediction System (COAMPS), *Oceanography*, *15*, 88–98.

Huang, N. E. (1979), On surface drift currents in the ocean, *J. Fluid Mech.*, *91*, 191–208.

Jenkins, A. D. (1987), Wind and wave induced currents in a rotating sea with depth-varying eddy viscosity, *J. Phys. Oceanogr.*, *17*, 938–951.

Jenkins, A. D. (1989), The use of a wave prediction model for driving a near-surface current model, *Dtsch. Hydrogr. Z.*, *42*, 133–149.

Kantha, L. H., and C. A. Clayson (2004), On the effect of surface gravity waves on mixing in the oceanic mixed layer, *Ocean Modell.*, *6*, 101–124.

Kudryavtsev, V. N., V. K. Makin, and B. Chapron (1999), Coupled sea surface-atmosphere model. 2: Spectrum of short wind waves, *J. Geophys. Res.*, *104*, 7625–7639.

Large, W. G., and S. Pond (1981), Open ocean momentum flux measurements in moderate to strong winds, *J. Phys. Oceanogr.*, *11*, 324–336.

Lentz, S. J., M. Fewings, P. Howd, J. Fredericks, and K. Hathaway (2008), Observations and a model of undertow over the inner continental shelf, *J. Phys. Oceanogr.*, *38*, 2341–2357.

Lewis, D. M., and S. E. Belcher (2004), Time-dependent, coupled, Ekman boundary layer solutions incorporating Stokes drift, *Dyn. Atmos. Oceans*, *37*, 313–351.

McWilliams, J. C., and E. Huckle (2006), Ekman layer rectification, *J. Phys. Oceanogr.*, *36*, 1646–1659.

McWilliams, J. C., P. P. Sullivan, and C.-H. Moeng (1997), Langmuir turbulence in the ocean, *J. Fluid Mech.*, *334*, 1–30.

Mellor, G. L. (2001), One-dimensional, ocean surface layer modelling: A problem and a solution, *J. Phys. Oceanogr.*, *31*, 790–809.

Noh, Y. (1996), Dynamics of diurnal thermocline formation in the oceanic mixed layer, *J. Geophys. Res.*, *26*, 2189–2195.

Noh, Y. (2004), Sensitivity to wave breaking and the Prandtl number in the ocean mixed layer model and its dependence on latitude, *Geophys. Res. Lett.*, *31*, L23305, doi:10.1029/2004GL021289.

Noh, Y., and H. J. Kim (1999), Simulations of temperature and turbulence structure of the oceanic boundary layer with the improved near-surface process, *J. Geophys. Res.*, *104*, 15,621–15,634.

Noh, Y., H. S. Min, and S. Raasch (2004), Large eddy simulation of the ocean mixed layer: The effects of wave breaking and Langmuir circulation, *J. Phys. Oceanogr.*, *34*, 720–733.

Pollard, R. T. (1973), Interpretation of near-surface current meter observations, *Deep Sea Res.*, *20*, 261–268.

Polton, J. A., D. M. Lewis, and S. E. Belcher (2005), The role of wave-induced Coriolis-Stokes forcing on the wind-driven mixed layer, *J. Phys. Oceanogr.*, *35*, 444–457.

Price, J. F., and M. A. Sundermeyer (1999), Stratified Ekman layers, *J. Geophys. Res.*, *104*, 20,467–20,494.

Price, J. F., R. A. Weller, and R. R. Schudlich (1987), Wind-driven ocean currents and Ekman transport, *Science*, *238*, 1534–1538.

Rascle, N., F. Ardhuin, and E. A. Terray (2006), Drift and mixing under the ocean surface: A coherent one-dimensional description with application to unstratified conditions, *J. Geophys. Res.*, *111*, C03016, doi:10.1029/2005JC003004.

Rascle, N., F. Ardhuin, P. Queffeulou, and D. Croizé-Fillon (2008), A global wave parameter database for geophysical applications. part 1: Wave-Current-Turbulence interaction parameters for the open ocean based on traditional parameterizations, *Ocean Modell.*, *25*(3–4), 154–171.

Santala, M. J. (1991), Surface referenced current meter measurements, Ph.D. thesis, WHOI-91-35, Woods Hole Oceanogr. Inst., Woods Hole, Mass.

Schudlich, R. R., and J. F. Price (1998), Observations of seasonal variation in the Ekman layer, *J. Phys. Oceanogr.*, *28*, 1187–1204.

Stramma, L., P. Cornillon, R. A. Weller, J. F. Price, and M. G. Briscoe (1986), Large diurnal sea surface temperature variability: Satellite and in situ measurements, *J. Phys. Oceanogr.*, *16*, 827–837.

Tarbell, S. A., N. J. Pennington, and M. G. Briscoe (1984), A compilation of moored current meter and wind recorder data: Vol. XXXV: Long-Term Upper Ocean Study (LOTUS) (mooring 764, 765, 766, 767, 770) May 1982–April 1983, *Tech. Rep. WHOI-84-86*, Woods Hole Oceanogr. Inst., Woods Hole, Mass. 02543.

Terray, E. A., M. A. Donelan, Y. C. Agrawal, W. M. Drennan, K. K. Kahma, A. J. Williams, P. A. Hwang, and S. A. Kitaigorodskii (1996), Estimates of kinetic energy dissipation under breaking waves, *J. Phys. Oceanogr.*, *26*, 792–807.

Terray, E. A., W. M. Drennan, and M. A. Donelan (2000), The vertical structure of shear and dissipation in the ocean surface layer, in *Proc. Symp. on Air–Sea Interaction*, pp. 239–245, Univ. of N. S. W., Sydney, Australia.

Tolman, H. L., B. Balasubramaniyan, L. D. Burroughs, D. V. Chalikov, Y. Y. Chao, H. S. Chen, and V. M. Gerald (2002), Development and implementation of wind-generated ocean surface wave models at NCEP, *Weather Forecasting*, *17*(4), 311–333.

Uppala, S. M., et al. (2005), The ERA-40 re-analysis, *Q. J. R. Meteorol. Soc.*, *131*, 2961–3012, doi:10.1256/qj.04.176.

Xu, Z., and A. J. Bowen (1994), Wave- and wind-driven flow in water of finite depth, *J. Phys. Oceanogr.*, *24*, 1850–1866.

F. Ardhuin and N. Rascle, Centre Militaire d'Océanographie, Service Hydrographique et Océanographique de la Marine, 13 rue du Chatellier, F-29609 Brest, France. (rascle@shom.fr)